Hindawi Publishing Corporation
Mathematical Problems in Engineering
Volume 2013, Article ID 749375, 7 pages
http://dx.doi.org/10.1155/2013/749375

Research Article

Calculation Formula Optimization and Effect of Ring Clearance on Axial Force of Multistage Pump

Chuan Wang, Weidong Shi, and Li Zhang

Research Center of Fluid Machinery Engineering and Technology, Jiangsu University, Zhen Jiang 212013, China

Correspondence should be addressed to Chuan Wang; wangchuanjsu@163.com

Received 4 July 2013; Revised 20 August 2013; Accepted 9 September 2013

Academic Editor: Yi-Chung Hu

Since overlarge axial force can damage the pump, accurate calculation formula of axial force on pump is very significant. The traditional formula is based on the assumption that the leakage amount of the pump is zero and the angular speed of fluid in the pump chamber rotates at half the impeller rotation's angular speed. In order to propose an accurate calculation formula, the whole flow fields of multistage pumps with three different ring clearances were calculated by using Computational Fluid Dynamics (CFD). The results indicate that the axial force on first-stage impeller is larger than that on the second. Along with the change of ring clearance, the static pressure distribution on the shroud of impeller changes at the same time, which leads to the value change of axial force. Meanwhile, angular speed of the fluid in the pump chamber is changing. Therefore, this research works out the reason why the error of traditional axial force calculation is large when the amount of leakage is relatively high. At last, an accurate calculation formula of axial force on pump is obtained through the verification of numerical simulation and experiment.

1. Introduction

The sectional multistage pump and high-head pump will generate huge axial force when running. Although balance devices are usually installed on the pump, balancing devices still may be damaged during operation due to inaccurate calculation of axial force, which in severe cases even results in accidents such as motor burn-outs [1–3]. Hence, accurate calculations of the axial force on the pump during the operation will directly affect the safety and reliability of pumps. The traditional formulas are based on the assumption as follows [4, 5]: the friction force of fluid in the pump is zero; the angular speed of fluid in the pump chamber rotates at half the impeller rotation's angular speed and the pressure distributes along the radial parabola; the leakage amount of the pump is zero.

However, with the operation of the pump, the ring clearance expands, the leakage amount changes, and the pressure distribution in the pump chamber changes also, which will influence the axial force [6, 7]. Therefore, the study of relationship between ring clearances and axial force has great engineering and academic value.

2. Calculation Formula of Axial Force

Figure 1 shows the distribution of axial force and pressure on the impeller in this paper. Some typical formulas of axial force are listed as follows.

The first recommended formula of axial force in the book of *Pump Manual* is as follows [8]:

$$\begin{aligned} A = {} & \left(r_{2a}{}^2 - r_{2i}{}^2\right)\pi\rho g\left[H_p - \frac{\omega^2}{16g}\left(r_{2i}{}^2 - r_h{}^2\right)\right] \\ & + \left(r_{2a}{}^2 - r_{2i}{}^2\right)\pi\rho g H_p - \left(r_{2i}{}^2 - r_{1a}{}^2\right)\pi\rho g \\ & \times\left[H_p - \frac{\omega^2}{16g}\left(r_{2i}{}^2 - r_{1a}{}^2\right)\right] - A_2, \end{aligned} \tag{1}$$

dynamic reaction:

$$A_2 = \rho Q_t\left(v_{m0} - v_{m3}\cos\alpha\right). \tag{2}$$

In the formulas, A is the axial force; ρ is density of liquid; g, acceleration of gravity; ω is impeller angular speed; r_{2a} is impeller radius of the front shroud; r_{2i} is impeller radius of

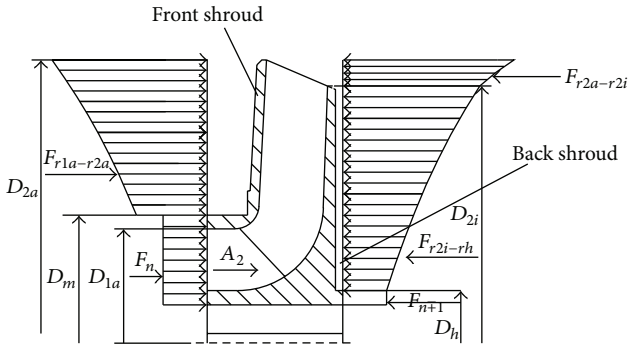

Figure 1: Distribution of axial force on one impeller.

the back shroud; r_h is hub radius; r_{1a} is ring radius; H_p stands for impeller head; Q_t is the flow rate; α is the included angle between the impeller outlet axial velocity and axial direction; v_{m0} and v_{m3} are the axial velocity at the inlet and outlet of impeller.

The second formula of axial force recommended by Pfleiderer is as follows [9]:

$$A = A_{1i} - A_{1a} + A_p - A_2, \tag{3}$$

the axial forces outside the back shroud:

$$A_{1i} = \gamma\pi\left(r_{2i}^2 - r_h^2\right)\left[H_{2i} - \frac{\omega^2\left(r_{2i}^2 - r_h^2\right)}{16g}\right], \tag{4}$$

the axial force inside the front shroud:

$$A_{1a} = \gamma\pi\left(r_{2a}^2 - r_{1a}^2\right)\left[H_{2a} - \frac{\omega^2\left(r_{2a}^2 - r_{1a}^2\right)}{16g}\right], \tag{5}$$

the axial component due to the axial clearance pressure:

$$A_p = \gamma\pi H_p\left(r_{2a}^2 - r_{1i}^2\right), \tag{6}$$

dynamic reaction:

$$A_2 = \rho Q_t\left(v_{m0} - v_{m3}\cos\alpha\right). \tag{7}$$

In the formulas: H_{2a} is the impeller head calculated through the streamline of the front shroud; H_{2i} is impeller head calculated through the streamline of the back shroud; γ is the unit weight of fluid.

The above two formulas are based on the assumption that the angular speed of fluid in the pump chamber rotates at half the impeller rotation's angular speed (ω). According to the early work of our research team, when the ring clearance of pump is 0.25 mm, the angular speed of fluid outside the front and back shroud is almost 0.45ω, while the angular speed of fluid outside the blade outlet is almost 0.65ω [6]. From the above, the third calculation formula of axial force on the impeller is as follows:

$$F = F_{r2a-r2i} + F_{r2i-rh} - F_{r1a-r2a} - A_2 - F_n, \tag{8}$$

Table 1: Geometrical parameters of pump.

Parameters	Names	Values
D_{2a}	Impeller outlet diameter of front shroud	119 mm
D_2	Average impeller outlet diameter	113.5 mm
D_m	Ring diameter	53.7 mm
D_{1a}	Impeller inlet diameter	48 mm
D_h	Hub diameter	22 mm
D_{2i}	Impeller outlet diameter of back shroud	108 mm
α	Included angle between the outlet axial velocity and axial direction	66.78°

Table 2: Calculated results.

Formula	First	Second	Third
F (N)	268.86	59.87	154.09

the axial force inside the front shroud:

$$F_{r2a\text{-}r2i} = \gamma\pi\left(r_{2a}^2 - r_{2i}^2\right)\left[H_{2a} - \frac{\omega^2 a^2\left(r_{2a}^2 - r_{2i}^2\right)}{4g}\right], \tag{9}$$

the axial forces outside the back shroud:

$$F_{r2a-rh} = \gamma\pi\left(r_{2i}^2 - r_h^2\right)\left[H_{2i} - \frac{\omega^2 b^2\left(r_{2i}^2 - r_h^2\right)}{4g}\right], \tag{10}$$

the axial force outside the front shroud:

$$F_{r1a-r2a} = \gamma\pi\left(r_{2a}^2 - r_{1a}^2\right)\left[H_{2a} - \frac{\omega^2 c^2\left(r_{2a}^2 - r_{1a}^2\right)}{4g}\right], \tag{11}$$

the axial force outside the ring:

$$F_n = \gamma\pi\left(r_{1a}^2 - r_h^2\right)p_1, \tag{12}$$

dynamic reaction:

$$A_2 = \rho Q_t\left(v_{m0} - v_{m3}\cos\alpha\right). \tag{13}$$

In the formulas F is the axial force; a, b, c, respectively, represent, the correction factor of circumferential speed of fluid outside the impeller front shroud, the correction factor of circumferential speed of fluid on oblique plane of blade, diameter and the correction factor of circumferential speed of fluid inside oblique plane of the impeller shroud; p_1 is the static pressure at the impeller inlet. Suppose that p_1 is the reference pressure and p_1 can be zero; so $F_n = 0$.

The axial force of one model pump will be calculated by using above three formulas, and the geometrical parameters of the pump are shown in Table 1.

At the rated condition, the rotation speed of pump n = 2850 r/min, the total head H = 65 m, and the flow rate Q = 20 m^3/h. The results calculated by three formulas are shown in Table 2. Due to the difference between the assumption and the actual situation, the axial forces calculated by above formulas are approximation. According to Table 2, the results differ greatly by above three formulas. Therefore, experiments are combined to verify the accuracy of these formulas.

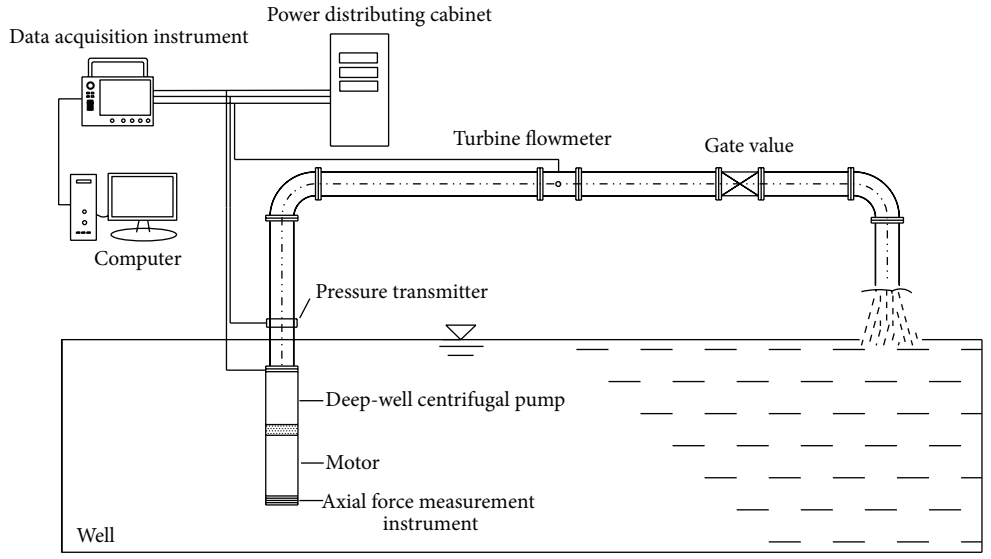

Figure 2: Test rig of open-type pump system.

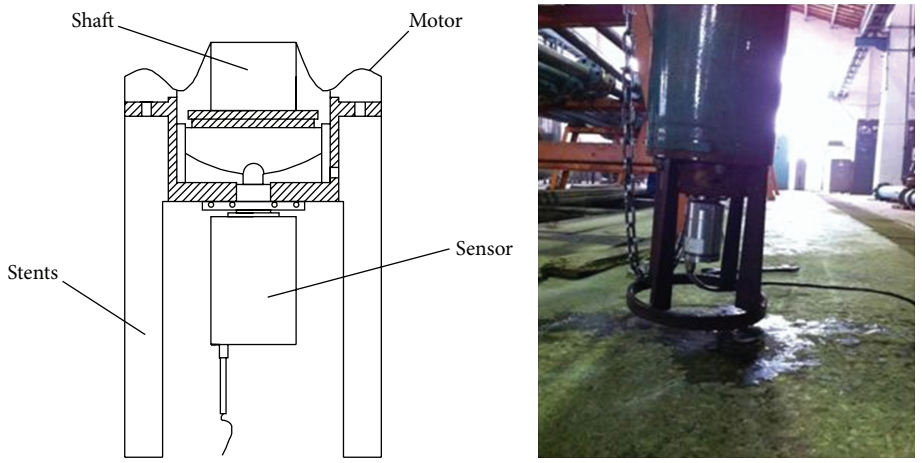

Figure 3: Axial force test equipment.

3. Test Measurement

3.1. Test Rig Setup. Experiments were done in an open-type pump system, which have the identification from Jiangsu Province of China. The test rig is composed of two parts, namely, the data acquisition system and the water circulation system [10]. The data acquisition system changes all kinds of physical quantities at different conditions, while the water circulation system supplies the necessary environment for centrifugal pump operation. The test rig is shown in Figure 2. A turbine flowmeter was used to measure the flow Q and the precision of turbine flowmeter is ±0.3%. Speed n is measured by a tachometer (PROVA RM-1500, Taiwan). During the experiment, only one dynamic pressure transmitters (CYG1401) was used to measure the outlet pressure. The precision of CYG1401 is ±0.2%. In order to capture the detailed axial force value, a pressure sensor was installed at the bottom of the motor's rotor, which connects an axial force measurement instrument, as shown in Figure 3, and its measurement error was reported as 0.2% by the manufacturer.

Table 3: Experimental axial force of one impeller.

Q (m^3/h)	12	16	20	24	28
F (N)	213.82	205.10	178.38	124.74	52.79

3.2. Experimental Results. Table 3 shows the experimental axial force of one impeller. From Table 3, when the flow rate is 20 m^3/h and the rotation speed of pump n = 2850 r/min, the experimental axial force of one impeller is 178.38 N. Compared with the experimental value and theoretical results calculated through three formulas, the axial force calculated

through the third formula is most close to the experimental value. That is because the third formula revises the angular speed of the liquid outside the front shroud and back shroud. The revised static pressure distribution should be more consistent to the static pressure distribution in the actual flow field. The axial force calculated through the first formula is the greatest, because in the first formula the static pressure outside the impeller exit of back shroud and oblique plane are taken to be equal to the static pressure outside the impeller exit of front shroud, which makes the calculated value much greater than the experimental value. The axial force calculated through the second the formula is much smaller than the experimental value. In the second formula, the static pressure outside the impeller exit of oblique plane is taken according to the middle streamline, and the static pressure outside the impeller exit of back shroud is taken according to the streamline of back shroud. The continuity of pressure change outside the impeller exit of oblique plane has not been taken into account, which is the cause of small axial force.

4. Numerical Calculation

4.1. Solid Modeling and Grid Meshing. The whole flowing parts of pump are composed of inlet section, ring, impeller, guide vane, and outlet section [11–14]. The model is respectively established and assembled together in Pro/E. Aiming at relationship between the axial force and different ring clearances, three pumps with different ring clearances of 0 mm, 0.25 mm, and 0.5 mm are established. This pump is one of multistage pumps, and the number of grids increases with the impeller series. Limited by computer and computing time, the two-stage pump is established in this paper, which can be seen in Figure 4. This mesh generation is completed by using special preprocessing software—Gambit, which is considered to be one of the best commercial CFD software preprocessor. In the whole model, unstructured tetrahedral mesh is used, and the mesh of impeller and guide vane can be seen in Figure 5.

4.2. Control Equations. In this paper, standard k-ε turbulence model control equations and SIMPLEC algorithm are used [15–17]. Besides, momentum, turbulent kinetic energy and turbulence dissipation rate all adopt second order upwind. Moreover, standard pressure item is selected. In order to accelerate convergence, various relaxation factors employ 0.3. The inlet and outlet of pump, respectively, adopt velocity inlet and outflow; the solid wall is not slip.

5. Numerical Results and Analysis

5.1. The Division of Axial Force. Usually the traditional calculation formula for axial force only considers the axial force on the outer surface of the impeller, not including the axial force on the inner surface of the impeller. The axial force on inner surface of impeller is regarded as internal forces. And it is considered that the total force of internal force is zero. This is acceptable in theory but difficult to understand and analyze. In contrast, it is easier to understand and analyze

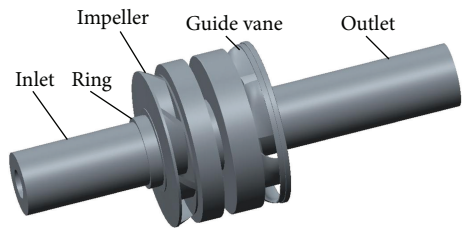

Figure 4: The two-stage pump.

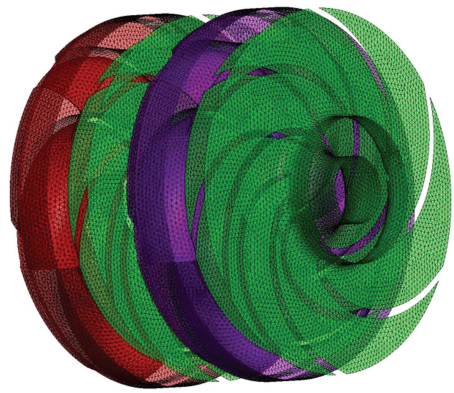

Figure 5: The grid of impeller and guide vane.

that the axial forces are the total axial components of forces on inner and outer surface of impeller. Therefore, the inside and outside surfaces of impeller are divided into the following sections:

$$F = \vec{F}_1 + \vec{F}_2 + \vec{F}_3 + \vec{F}_4 + \vec{F}_5 + \vec{F}_6. \quad (14)$$

In the formulas, the axial force on the outer surface of the impeller front shroud F_1 (excluding the seal faces); the axial force on the outer surface of the impeller back shroud F_2 (including the hub); the axial force on the annular region from outer diameter to inner diameter of impeller ring F_3; the axial force on the impeller inner surface of front and back shroud F_4 (including the hub); the axial force of blade surface F_5; the axial force on oblique part of the blade outlet edge F_6.

Figure 6 indicates the axial force of first-stage impeller and second-stage impeller in different flow rate with three ring clearances. The performance curve shows that the head is high at small flow rate condition, resulting in high static pressure on the front shroud, back shroud, and the impeller inner surface. The axial forces on the front and back shroud increase certainly. The axial force difference on the front and back shroud accounts for a large part in the composition of axial force. Therefore, the axial force at small flow rate condition is great. The reaction forces increase at large flow rate condition, but the axial force caused by the reaction force only accounts for adequately small part in the total axial force.

Figure 7 points out the comparison between the experimental values and numerical calculation values. From Figure 7, the experimental results are relatively close to the numerical simulation results at the design flow rate. The flow in the impeller is very complex at the non-design

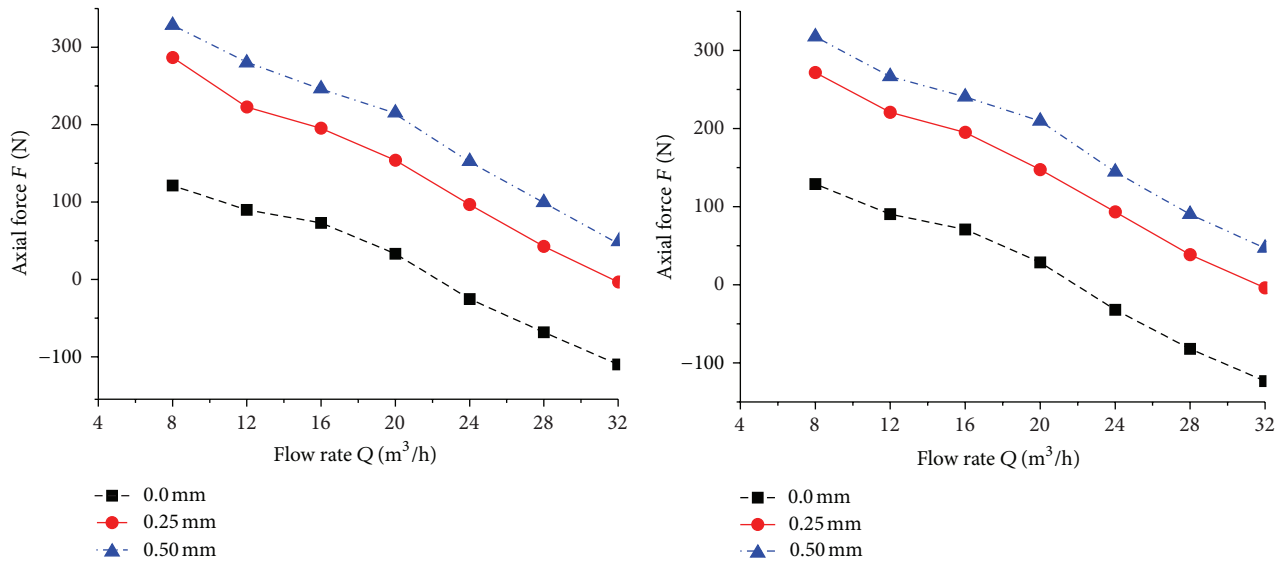

(a) Axial force of first-stage impeller

(b) Axial force of second-stage impeller

Figure 6: F-Q curve of primary and secondary impeller with different ring clearances.

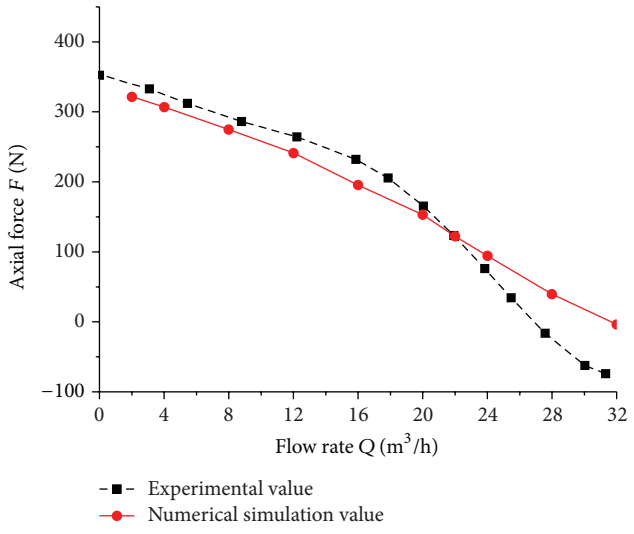

Figure 7: Comparison of experimental values and the numerical simulation values.

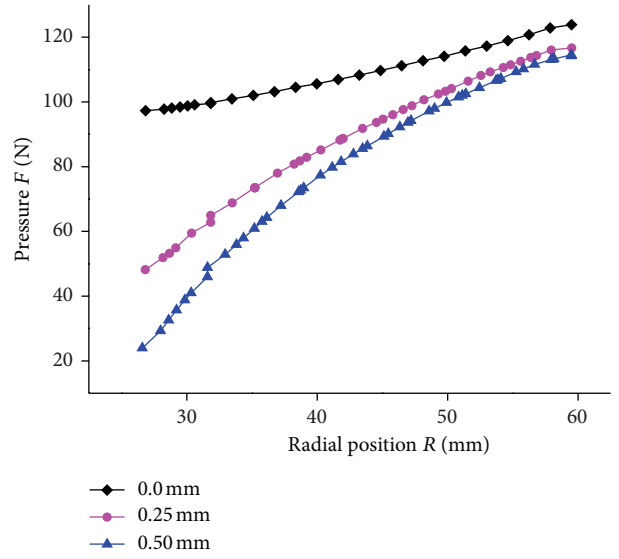

Figure 8: Radial static pressure of front shroud of impeller.

working conditions, so the calculation can not reflect the real flow. However, the trend of calculated value at nondesign condition is consistent with the experimental trends.

This paper focuses on analyzing the relationship between the axial force and the ring clearance. Table 3 shows the calculated value of each component of axial force on the impellers with three ring clearances. According to Table 4, the values of F_3 on the corresponding impellers with different ring clearances are different, while the other values are very close to each other. The axial force on one impeller with the ring clearance of 0.5 mm is 60 N larger than that with the ring clearance of 0.5 mm, which shows that a reasonable ring clearance should be selected.

Figure 8 shows the radial static pressure of front shroud of impeller. According to Figure 8, the static pressure on the front shroud decreases along the radial position, and larger ring clearance brings about faster decline of static pressure. Axial force on the front shroud is obtained by numerical integration of static pressure on the surface, and the direction of axial force on the front shroud and total axial force on the impeller are in the opposite. Therefore, smaller ring clearance determines lower total axial force.

5.2. Angular Distribution of the Fluid in Pump Chamber. This pump is a multistage pump. In order to reduce the maximum

Table 4: Calculated value of each component of axial force on the impellers with three ring clearances.

Clearance		F_1 (N)	F_2 (N)	F_3 (N)	F_4 (N)	F_5 (N)	F_6 (N)	F (N)
0.0 mm	First stage	798.075	−974.2899	−0.4571	24.2695	−0.2887	185.956	73.0531
	Second stage	1832.09	−2017.003	−57.217	48.0199	−20.43	237.215	70.8216
0.25 mm	First stage	790.095	−842.824	−1.0523	23.8369	−0.3041	182.096	151.847
	Second stage	1807.82	−1869.446	−50.253	47.1561	−19.965	232.105	147.418
0.5 mm	First stage	782.72	−770.935	−0.2441	23.3823	−0.0271	180.348	215.245
	Second stage	1791.75	−1791.943	−47.195	46.4717	−19.759	230.165	209.487

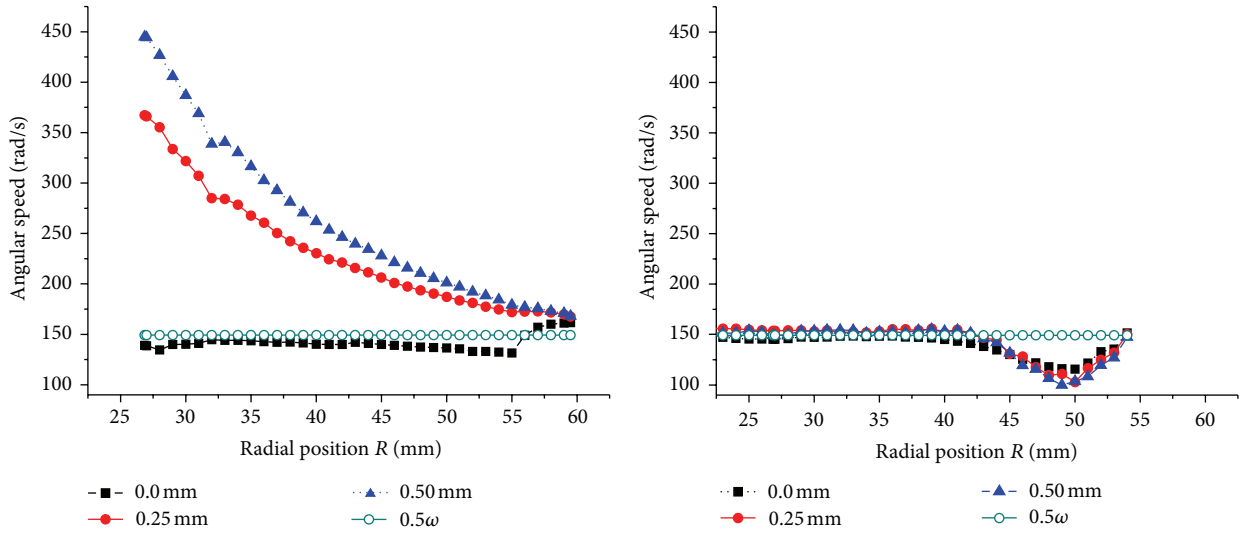

(a) In the front pump chamber

(b) In the back pump chamber

Figure 9: Radial distribution of angular speed of the liquid in the second pump chamber.

shaft power, the outlet placed angle of guide vane is usually less than 90 degree. When the liquid comes out from the first guide vane and goes into the second impeller, there is certain angular speed in the liquid. In other words, the liquid is preswirled before entering the second impeller. In this paper, because the flow field of the second-stage pump is more representative in multistage pump, only the angular speed of the liquid in the second-stage pump chamber is shown in Figure 9 (ω: angular speed of the impeller). As can be seen from Figure 9, the radial distribution of angular speed is not equal to half the rotating speed of the impeller. The angular speed decreases along the radial direction. According to the angular momentum conservation law, greater radius means smaller angular speed. The angular speed of the fluid in the impeller exit is greater than 0.5ω because it is driven by rotation of the exit of impeller blade. Document [18] simplifies the liquid flow in the pump chamber as the rotation of enclosed cavity around the fixed axis. From the surface of pump body to the surface of rotating impeller, the whole flow passage is divided into pump body boundary layer, outflow layer, core area, and impeller boundary layer. When the ring clearance is 0 mm, most of the fluid in the core area of pump chamber makes approximately rigid motion with 40%–50% ω, which accords with the document [6] that the angular speed of the outside of impeller cover is revised as 0.45ω. With the broadening of ring clearance, the average angular speed of liquid in the same radius of the front pump chamber also increases and in the core area increases to more than 0.55ω. Since it is assumed to be no leakage in the back pump chamber, with the increase of ring clearance, the angular speed distribution of fluid in the back pump chamber remains almost the same. Therefore, when the ring clearance increases, the angular speed of liquid enhances and the circumference angular speed correction coefficient also increases, for the flow condition of the liquid changes in the front part of pump chamber. So the force of the front shroud $F_{r1a-r2a}$ reduces. Because the force direction of $F_{r1a-r2a}$ opposites the stated positive direction of force, the total force F increases.

6. Conclusion

The model pumps with three different ring clearances were simulated, respectively, through CFD. The results indicate that the axial force in the front shroud improves with the increase of ring clearance. The increase of static pressure in the front shroud on the same radius is the main reason enhancing axial force. When the ring clearance is 0 mm, the angular speed of liquid in the pump chamber is 0.4-0.5ω. With the increase of ring clearance, in the front pump

chamber the angular speed of liquid improves and the correction coefficient of circumference angular speed outside the front shroud also increases. At this point there may be large errors to use traditional formula for calculating axial force. The experimental results are relatively close to the numerical simulation results at the design flow rate. And numerical calculation can be used as an effective method to verify axial force because of its high accuracy and convenience.

Acknowledgments

This research was supported by the Priority Academic Program Development of Jiangsu Higher Education Institutions, the Scientific and Technological Innovation team Project of College in Jiangsu Province (no. [2009]10), and the National Natural Science Foundation of China (Grant nos. 51109093 and 51279069).

References

[1] D. Childs, "Fluid-structure interaction forces at pump-impeller-shroud surfaces for axial vibration analysis," *ASME Journal of Vibration and Acoustics*, vol. 113, no. 1, pp. 108–115, 1991.

[2] Y. A. Kazakov and A. A. Pelinskii, "Experimental investigation of the axial force in a submersible, electric well pump," *Chemical and Petroleum Engineering*, vol. 6, no. 3, pp. 262–263, 1970.

[3] D. O. Baun and R. D. Flack, "Plexiglas research pump with calibrated magnetic bearings/load cells for radial and axial hydraulic force measurement," *ASME Journal of Fluids Engineering*, vol. 121, no. 1, pp. 126–132, 1999.

[4] F. G. Johann, *Centrifugal Pumps*, Springer, New York, NY, USA, 2008.

[5] J. J. Karassik and R. Carter, *Centrifugal Pumps*, F. W. Dodge, New York, NY, USA, 1980.

[6] W. Lu, Q. Li, W. Shi et al., "Experiment for axial thrust of shortened impeller back shroud," *Drainage and Irrigation Machinery*, vol. 26, no. 1, pp. 1–5, 2008.

[7] Y. Choi, J. Kurokawa, and J. Malsui, "Performance and internal flow characteristics of a very low specific speed centrifugal pump," *ASME Journal of Fluids Engineering*, vol. 128, no. 2, pp. 341–349, 2006.

[8] X. Guan, *Modern Pumps Theory and Design*, Astronautic Publishing House, Beijing, China, 2011.

[9] C. Pfleiderer, *Stromugsmasch*, Springer, Berlin, Germany, 1964.

[10] B. Helmut, J. Helmut, Y. Hoi et al., "Numerical simulation of low specific speed American petroleum institute pumps in part-load operation and comparison with test rig results," *ASME Journal of Fluids Engineering*, vol. 134, no. 2, Article ID 024501, 9 pages, 2012.

[11] L. Zhou, W. Shi, W. Lu et al., "Numerical investigations and performance experiments of a deep-well centrifugal pump with different diffusers," *ASME Journal of Fluids Engineering*, vol. 134, Article ID 0711002, 8 pages, 2012.

[12] W. Shi, C. Wang, Q. Si et al., "Numerical calculation of stainless steel stamping well pump based on regression orthogonal test," *International Journal of Comprehensive Engineering*, vol. 1, no. 1, pp. 39–49, 2012.

[13] H. Wang, W. Shi, W. Lu, L. Zhou, and C. Wang, "Optimization design of deep well pump based on latin square test," *Transactions of the Chinese Society of Agricultural Machinery*, vol. 41, no. 5, pp. 56–63, 2010.

[14] W. Shi, Q. Li, and W. Lu, "Estimation and experiment of axial thrust in centrifugal pump based on CFD," *Transactions of the Chinese Society of Agricultural Machinery*, vol. 40, no. 1, pp. 60–63, 2009.

[15] D. Zhang, W. Shi, B. Chen et al., "Unsteady flow analysis and experimental investigation of axial-flow pump," *Journal of Hydrodynamics B*, vol. 22, no. 1, pp. 35–44, 2010.

[16] J. González, C. Santolaria, and F. Castro, "Numerical model for the unsteady flow behaviour inside a double suction pump," in *Proceedings of the 4th ASME/JSME Joint Fluids Engineering Conference (FEDSM '03)*, pp. 1149–1155, Honolulu, Hawaii, USA, July 2003.

[17] K. M. Guleren and A. Pinarbasi, "Numerical simulation of the stalled flow within a vaned centrifugal pump," *Proceedings of the Institution of Mechanical Engineers C*, vol. 218, no. 4, pp. 425–435, 2004.

[18] Y. Senoo and H. Hayami, "An analysis on the flow in a casing induced by a rotating disk using a four layer flow model," *ASME Journal of Fluids Engineering*, vol. 98, no. 2, pp. 192–198, 1976.